International Journal of Nanomedicine

Dovepress
Taylor & Francis Group

Open Access Full Text Article

ORIGINAL RESEARCH

RETRACTED ARTICLE: $_{h}CeO_2$@CA-074Me Nanoparticles Alleviate Inflammation and Improve Osteogenic Microenvironment by Regulating the CTSB-NLRP3 Signaling Pathway

Zhaojun Niu[1,2], Xiaomin Xia[1,2], Zhimin Zhang[1], Jie Liu[1,2], Xue Li[1,2]

[1]Department of Stomatology, The Affiliated Hospital of Qingdao University, Qingdao University, Qingdao, People's Republic of China; [2]School of Stomatology, Qingdao University, Qingdao, People's Republic of China

Correspondence: Jie Liu; Xue Li, Email 18661801995@163.com; lixue@qdu.edu.cn

Background: It is well established that the interaction between osteogenesis and inflammation can impact bone tissue regeneration. The use of nanoparticles to treat and alleviate inflammation at the molecular level has the potential to improve the osteogenic microenvironment and serve as a therapeutic approach.

Methods: We have synthesized new hollow cerium oxide nanoparticles and doped with cathepsin B inhibitor (CA-074Me) to create novel $_{h}CeO_2$@CA-074Me NPs. We characterized the surface morphology and physicochemical properties of $_{h}CeO_2$@CA-074Me NPs. Macrophage RAW 264.7 was cultured with $_{h}CeO_2$@CA-074Me NPs using *P. gingivalis*-LPS (*P.g*-LPS) stimulation as a model of inflammation. RT-PCR and Western blot analysis was employed to evaluate the effects of $_{h}CeO_2$@CA-074Me NPs on macrophage phenotype and the CTSB-NLRP3 signaling pathway. To further investigate the inflammatory osteogenic microenvironment, MC3T3-E1 cells were cultured with *P.g*-LPS to create simulated in vitro osteogenic conditions under inflammation. The cells were then co-cultured with $_{h}CeO_2$@CA-074Me NPs for 7, 14, and 21 d. The osteogenic ability was evaluated using ALP staining, ALP quantitative analysis, alizarin red staining, and RT-PCR analysis.

Results: Findings clearly demonstrated that $_{h}CeO_2$@CA-074Me NPs could effectively reduce the production of ROS and inhibited CTSB-NLRP3 signal pathway, thereby significantly attenuating the damage caused by the cellular inflammatory response. $_{h}CeO_2$@CA-074Me NPs could also influence the polarization of macrophages towards anti-inflammatory M2 phenotype. Additionally, results confirmed that $_{h}CeO_2$@CA-074Me NPs could inhibit inflammation and ameliorate osteogenic microenvironment, thus promoting the osteogenesis of MC3T3-E1 cells.

Conclusion: The synthetic $_{h}CeO_2$@CA-074Me NPs could able to modify the osteogenic microenvironment under inflammatory conditions by simultaneously inhibiting the CTSB-NLRP3 signaling pathway and regulating the macrophage phenotype through their ability to scavenge ROS. Based on these findings, our study may offer a promising approach for managing inflammatory bone damage.

Keywords: cerium oxide nanoparticles, CTSB, NLRP3, inflammation, bone regeneration, osteogenic microenvironment

Introduction

The process of natural bone healing is similar to the process of bone development, involving various physiological events such as inflammation, vascular regeneration, calcification, and bone remodeling. Additionally, the coordinated action of inflammatory cells and those involved in bone healing is crucial for the formation, repair, and remodeling of healthy bones.[1] Bone regeneration is a complex process that involves interactions between the formation of new bone tissue and the inflammatory response.[2] The immune system plays a vital role in maintaining bone health by stimulating the mineralization of bone-forming cells, forming osteoclasts, and participating in the modeling and remodeling phases, ultimately maintaining overall osseous tissue homeostasis.[3] Given the established link between inflammation and bone

Received: 17 October 2024
Accepted: 16 December 2024
Published: 6 January 2025

resorption, there has been a growing interest in strategies aimed at enhancing the osteogenic microenvironment through anti-inflammatory approaches.[4]

Inflammation is crucial in the mineralization of osteoblasts, as it is necessary for osteogenesis to occur. Macrophages, the first line of defense against pathogen infection during inflammation, can have different functions depending on the physiological or pathological conditions: they can either have pro-inflammatory macrophage (M1 phenotype) or an anti-inflammatory macrophage (M2 phenotype).[5] It has been demonstrated that the enhanced M2 phenotype may limit inflammation and improve the osteogenic microenvironment. On the other hand, the M1 phenotype has been shown to exacerbate inflammation and disrupt bone-biomaterial integration. The polarization of macrophage plays a significant role in bone formation. Activation of inflammatory macrophage can increase local expression of RANKL, thereby promoting osteoclasts differentiation in bone tissue.[6] In contrast, anti-inflammatory macrophage aid in resolving inflammation and regenerating bone tissue by releasing anti-inflammatory mediators.[7] Additionally, M2 macrophages help remove apoptotic osteoblasts and contribute to bone formation.[8] The imbalance between pro-inflammatory and anti-inflammatory macrophage is one of the factors that disrupts bone tissue formation. Therefore, changing the phenotype of macrophage from pro-inflammatory to anti-inflammatory can effectively improve the bone microenvironment and enhance bone regeneration.

In the study of macrophages regulation of the immune response, researchers discovered that both cathepsin B (CTSB) and NLRP3 inflammasomes have pro-inflammatory effects.[9] CTSB has been implicated in various processes such as inflammation, cancer metastasis, and cell death.[10] In fact, several studies have suggested a role for CTSB in bone remodeling: including its involvement in perpetuating osteoarthritis and inhibiting bone regeneration.[10–13] Similarly, the activation of NLRP3 is triggered by inflammatory processes or tissue damage, ultimately leading to caspase-1 activation and the induction of pyroptosis. The literature likewise indicates that NLRP3-mediated cellular pyroptosis is logically linked to inflammatory bone destruction and infectious bone damage, and plays a role in the pathology of periodontitis.[14] Surprisingly, studies have shown that the specific inhibitor of CTSB, such as cathepsin B inhibitor (CA-074Me), can suppress the activation of NLRP3 inflammasomes. This suggests that CTSB can affect NLRP3 in several ways, including reducing the expression of the NLRP3 gene and inhibiting the activation of NLRP3.[15] Additionally, macrophages stimulated by inflammation have been observed to express high levels of CTSB and NLRP3. Therefore, modulating the immune response of macrophage and inhibiting the CTSB/NLRP3 signaling pathway may be an effective approach to suppressing inflammation and improving the osteogenic microenvironment.

Although natural enzymes are highly active and selective, they are easily inactivated and difficult to store.[16] CeO_2 NPs are a powerful artificial oxidase that mimics the activity of catalase (CAT) and superoxide dismutase (SOD) to attenuate and eliminate ROS production.[17] The reversible Ce^{3+}/Ce^{4+} redox potentials enables CeO_2 NPs to emulate the behaviour of SOD and CAT through the presence of a substantial number of surface oxygen vacancies. It has been suggested that the antioxidant mechanism of CeO_2 NPs is closely related to the presence of Ce^{3+}, which contributes to the formation of oxygen vacancies.[18] This indicates that a higher Ce^{3+}/Ce^{4+} ratio on the CeO_2 NPs surface increases the concentration of defects and oxygen vacancies in the lattice, resulting in higher antioxidant enzyme mimetic activity.[19] The Ce^{3+}/Ce^{4+} interconversion on the surface of CeO_2 NPs also enable them decrease the release of pro-inflammatory mediators, such as IL-6 and IL-1β. Additionally, due to their Ce^{3+}/Ce^{4+} redox potentials, CeO_2 NPs are considered effective scavengers of ROS, which play a critical role in maintaining bone homeostasis. Moreover, it was observed that a high level of Ce^{4+} in CeO_2 NPs promoted the proliferation of osteoblast cells MG63, while a high level of Ce^{3+} in CeO_2 NPs inhibited the growth of human mesenchymal stem cells MG63.[20]

Some studies suggested that CeO_2 NPs can promote osteogenic differentiation by stimulating the differentiation of M2 macrophage and mesenchymal stem cells. Study has shown that the osteogenic differentiation capability of BMSCs is directly proportional to the Ce^{4+}/Ce^{3+} ratio on titanium surfaces. A higher Ce^{4+}/Ce^{3+} ratio also promotes the polarization of RAW264.7 macrophage toward the M2 phenotype, particularly increasing the proportion of healing-associated M2 macrophage and the secretion of anti-inflammatory cytokines.[21,22] This suggested that the valence states of CeO_2 NPs could effectively modulate both the osteogenic potential of stem cells and the M2 polarization of macrophage. These effects collectively contribute to improved outcomes in new bone formation and osseointegration. While CeO_2 NPs possess antioxidant properties, the cytotoxicity of different types of CeO_2 NPs varies depending on

their chemical function, shape, size, aggregation status, and other properties.[23] CeO_2 NPs are expected to garner increasing interest in future research. It will be essential for investigators to explore the pathology and toxicology of CeO_2 NPs from a pathogenesis perspective to identify the most suitable types of CeO_2 NPs for human applications.

In conclusion, we have developed a new nanosystem, $_hCeO_2$@CA074Me NPs, by loading CTSB specific inhibitors CA-074Me with hollow CeO_2 NPs ($_hCeO_2$ NPs). Our study aimed to investigate whether $_hCeO_2$ NPs could improve the osteogenic microenvironment under inflammatory conditions by modulating macrophage phenotype and inhibiting the CTSB-NLRP3 signaling axis (Scheme 1). Our specific experiments included: (1) Development of $_hCeO_2$@CA-074Me NPs and characterization of its physical and chemical properties. (2) Evaluation of the biocompatibility of $_hCeO_2$@CA-074Me NPs. (3) Assessment of the inhibitory effect of $_hCeO_2$@CA-074Me NPs on macrophage inflammation factor secretion and its impact on the CTSB-NLRP3 pathway. (4) Evaluation of the effect of $_hCeO_2$@CA-074Me NPs on osteogenic status under *P. gingivalis*-LPS (*P.g*-LPS) stimulation. The experimental results demonstrated that $_hCeO_2$@CA-074Me NPs exhibited favorable biocompatibility and were capable of effectively scavenging ROS. Furthermore, they were able to enhance the osteogenic microenvironment under inflammatory conditions by simultaneously inhibiting the CTSB-NLRP3 signaling pathway and regulating the macrophage phenotype through their ability to scavenge ROS. Based on these findings, our study may offer a promising approach for managing inflammatory bone damage.

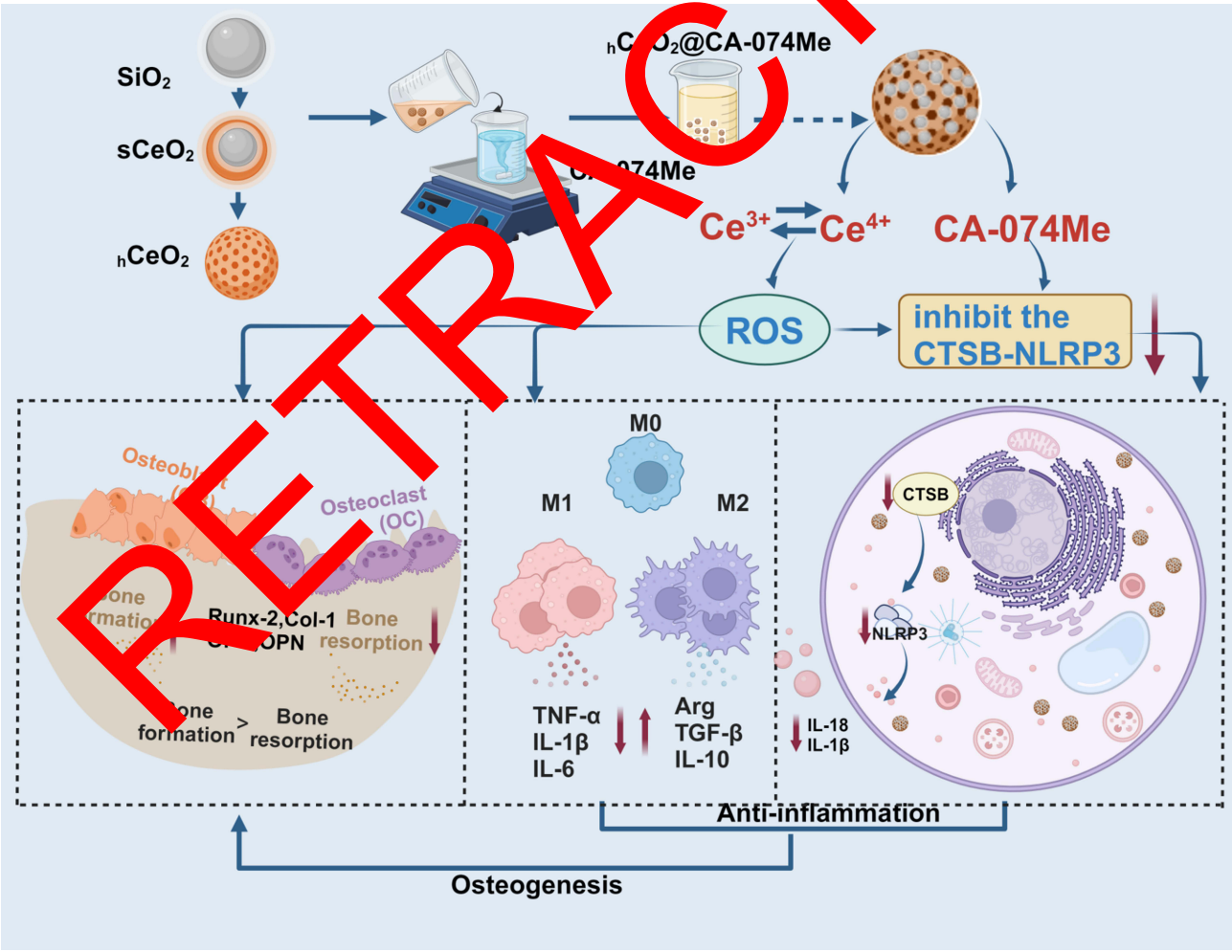

Scheme 1 The synthesis process of $_hCeO_2$@CA-074Me nanoparticles and their capability to ameliorate the osteogenic microenvironment under inflammatory conditions by modulating macrophage M2 phenotype polarization and suppressing the CTSB-NLRP3 signaling pathway.

https://doi.org/10.2147/IJN.S389156

Materials and Methods

Materials and Reagents

Polyvinylpyrrolidone (PVP) was purchased from Ourchem (Shanghai, China). Tetraethoxysilane (TEOS) and cerium (III) nitrate hexahydrate [$Ce(NO_3)_3{\cdot}6H_2O$] were obtained from Macklin (Shanghai, China). Hexamethylenetetramine (HMTA) and sodium hydroxide (NaOH) were purchased from Hushi (Shanghai, China). Counting Kit-8 and CA-074Me were obtained from Dalian Meilun. AM/PI Double Staining Kit was purchased from Beyotime Biotechnology (Shanghai, China). ABclonal (Wuhan, China) supplied ABScript III RT Master Mix and SYBR Green Fast qPCR Mix. CathepsinB Rabbit mAb was purchased from Cell Signaling Technology (Boston, MA, USA). Beta-actin polyclonal antibody and goat anti-rabbit IgG were purchased from Elabscience Biotechnology Co.Ltd. (Wuhan, China). Reagent-grade water was obtained from ultra-pure water system (Ulupure, Chengdu, China) in all experiments. All other reagents were of analytical grade without further purification.

Preparation of Hollow CeO_2 ($_hCeO_2$) NPs

The synthesis of hollow CeO_2 ($_hCeO_2$) NPs was referred to a previous literature.[24]

Preparation of Silica (SiO_2) NPs as a Template: 30 mL of absolute ethanol, 5 mL of 4 mol/L ammonia solution, and 4 mL of deionized water were put into an oil bath and mixed. When the above-mentioned solution was heated to 60°C, the mixture of 5 mL TEOS and 20 mL of absolute ethanol was slowly dripped into the mixture. The mixture was stirred at 60°C for 4 h. After cooling to room temperature, the mixture was washed three times with ethanol and dried under vacuum at 60°C to obtain silica (SiO_2) NPs.

Preparation of SiO_2@CeO_2 Core–Shell ($sCeO_2$) NPs: 0.1 g silica and 1 g PVP were added to 40 mL of deionized water. When the oil bath was heated to 75°C, 5 mL of 0.5 mmol cerium nitrate and 5 mL of 0.5 mmol HMTA were added in turn. The mixture was stirred at 95°C for 2 h, washed and centrifuged three times after cooling, and dried to obtain SiO_2@CeO_2 core–shell ($sCeO_2$) NP precursors. The $sCeO_2$ NP precursors were heated to 600°C at 5°C/min for 2 h, and then heating was naturally dropped to room temperature to obtain $sCeO_2$ NPs.

Preparation of $_hCeO_2$ NPs: 0.1 g $sCeO_2$ NPs was dispersed in 40 mL of 2 mol/L sodium hydroxide and stirred for 24 h, centrifuged, washed three times with ethanol, and dried to obtain $_hCeO_2$ NPs.

Preparation of $_hCeO_2$@CA-074Me NPs

The safe concentration of $_hCeO_2$ NPs was determined to be 50 μg/mL using CCK8, and the optimal dosing concentration for CA-074Me was selected based on literature reviews.[25,26] Masses of 50 μg/mL $_hCeO_2$ NPs were weighed and added to a 100 μM CA-074Me solution. After stirring for 24 h, the precipitate obtained consisted of $_hCeO_2$@CA-074Me NPs.

Material Characterization and Physical Properties

The surface morphology of the nanoparticles was observed using transmission electron microscopy (HT7700, Japan), and particle size analysis of electron microscopy images of $_hCeO_2$ NPs was performed using Image J. Elemental analysis of nanomaterials was carried out by X-ray diffraction (Xtalab Synergy, Netherlands) and comparison with standard mapping. Analysis of the surface chemical composition and elemental valence of nanomaterials were determined by X-ray photoelectron spectroscopy (Smart Lab 3KW, Japan). Functional groups in the nanomaterials were determined by Fourier transform infrared (FTIR, Thermo Fisher) analysis, with spectra recorded in the range of 4000 to 600 cm^{-1}. The resulting FTIR spectrum is a graph of transmittance vs Wavenumber (cm^{-1}). The spectra were analysed using Origin software for the purposes of functional group analysis and peak identification. Nanoparticle Tracking Analysis and Dynamic Light Scattering (DLS) were carried out in suspensions. The $_hCeO_2$ and $_hCeO_2$@CA-074Me NPs were synthesised in deionised water. Following a 5 min sonication period, 1 mL of a clean, homogeneous, transparent sample devoid of any precipitation was transferred to a clean square cuvette manufactured from optical translucent disposable plastic for subsequent DLS and Z-potential measurements. The zeta potentials of nanoparticles were measured by Zetasizer (Malvern Zetasizer Nano ZS90) DLS method. The zeta potential and average particle size of nanoparticles were obtained by analysis in triplicate, take the average value.

SOD, CAT, and T-AOC Enzyme Mimic Activity

In order to evaluate the antioxidant properties of $_{h}CeO_2$@CA-074Me NPs, we employed an enzyme calibrator (Elx800, Bio Tek, USA) to measure their superoxide dismutase (SOD), catalase (CAT), and total antioxidant (T-AOC) capacities. The SOD, CAT, and T-AOC enzyme mimetic activities of $_{h}CeO_2$ and $_{h}CeO_2$@CA-074Me NPs were quantified using the respective assay kits from Solebo (China) for SOD, CAT, and T-AOC.

The reagents were thoroughly mixed in accordance with the instructions provided and subsequently divided into three distinct groups: a test group, a control group, and two blank groups. The $_{h}CeO_2$ and $_{h}CeO_2$@CA-074Me NPs were added to the test and control groups for 30 min of immersion in a 37°C water bath, after which the absorbance values at 560 nautical miles were recorded as test, control, blank 1 and blank 2, respectively. The inhibition rate and SOD activity were then calculated based on the aforementioned values.

The working solution for the CAT assay was incubated at 37°C for 10 min, after which the aforementioned liquids were added to the $_{h}CeO_2$ and $_{h}CeO_2$ @CA-074Me NPs, respectively. Following the mixing process, the absorbance value at 240 nm was immediately measured, and then the absorbance value after one minute was measured. The CAT activity was subsequently calculated from the absorbance value.

The total antioxidant capacity of the samples was calculated by determining the quantity of Fe^{3+}-TPTZ reduced to Fe^{2+}-TPTZ in an acidic environment. The $_{h}CeO_2$ and $_{h}CeO_2$ @CA-074Me NPs were combined with 180 μL of the working solution and 18 μL of distilled water. After 10 min of reaction at room temperature, the absorbance value at 593 nm was determined. The working solution, devoid of nanoparticles, was combined with distilled water for a period of 10 min, subsequently incorporated into the formulation, and the absorbance value at 593 nm was ascertained in order to determine the total antioxidant capacity.

Determination of Intracellular ROS

Reactive oxygen species (ROS) were quantified in lipopolysaccharide (LPS) and nanoparticle-treated cells using a ROS assay kit (Beyotime, Shanghai, China). RAW 264.7 cells were inoculated into 6-well plates at a density of 3×10^4 cells per well and randomly assigned to one of five groups. The first group served as a blank control. The second group was treated with *P.g*-LPS (1 μg/mL) for 4 h to establish an in vitro inflammatory model.[27] The third group was treated with LPS for 4 h, followed by a 24 h treatment with CA-074Me (100 μM). Groups 4 and 5 were treated with LPS for 4 h, after which safe $_{h}CeO_2$ and $_{h}CeO_2$@CA-074Me NPs were added. The $_{h}CeO_2$ and $_{h}CeO_2$@CA-074Me NPs were maintained for a period of 24 h. The medium containing nanoparticles was then replaced with serum-free medium supplemented with 10 μM DCFH-DA and incubated at 37°C for 30 min. The cells were then washed with serum-free medium three times and observed under an inverted fluorescence microscope.

Cell Culture

Mouse leukemia cell monocyte macrophage (RAW264.7) were purchased from American Type Culture Collection (ATCC, Manassas, VA, USA) and cultured in Dulbecco's modified Eagle's medium (DMEM) with 10% fetal bovine serum (FBS). The L929 cell line was purchased from ScienCell (San Diego, CA, USA) and cultured in DMEM with 10% FBS, 10,000 U/mL penicillin, and 10 mg/mL streptomycin. MC3T3-E1 cells were purchased from American Type Culture Collection (ATCC, Manassas, VA, USA) and cultured in DMEM containing 10% FBS, 10,000 U/mL penicillin, and 10 mg/mL streptomycin. Cells were passaged when the density reached 80% - 90%. All cell lines were cultured at 37°C in an incubator with 5% CO_2.

Cytotoxicity Assay

Cytocompatibility Test of $_{h}CeO_2$ NPs with L929 and MC3T3-E1 Cells

The cytotoxicity of the nanoparticles was evaluated by using Cell Counting Kit-8 (Shanghai St Er), and the safe concentration was screened for subsequent experiments. L929 cells and MC3T3-E1 cells were seeded into 96-well plates at 5×10^3 cells per well. After cell adhesion, different concentrations (0, 5, 10, 20, 30, 40, 50, 100, 150 and 200 μg/mL) of nanoparticles were added to the culture for 24, 48, and 72 h. The medium-containing nanoparticles were removed

and the cells were washed three times with PBS. Then, 10% CCK8 reagent was added, and the cells were incubated in an incubator at 37°C for 1 h in the dark. Absorbance at 450 nm was then determined using a microplate reader (Bio-Tek, Winooski, VT, USA). Five parallel wells were set up for each group, and the experiment was repeated three times. After treatment of the nanoparticles, the L929 cells were washed three times with PBS and incubated with calcein-AM and PI for 30 min before being observed under a fluorescence inverted microscope.

Hemolysis Test of $_{h}CeO_2$ NPs

For the hemolysis assay, fresh blood was obtained from three six-week-old male BALB/c mice, and anticoagulant and saline were added to test the hemolytic potential of $_{h}CeO_2$ NPs in vitro. Blood diluted with distilled water was used as a positive control, and blood diluted with saline was used as a negative control. The cells were incubated at 37°C for 4 h and centrifuged at 2500 RPM for 10 min, the supernatant was removed, and the absorbance at 545 nm was recorded using a microplate reader. Hemolysis rates were calculated according to the following formula:

$$\text{Hemolysis rate} = \left(OD_{exper} - OD_{negative}\right) / \left(OD_{positive} - OD_{negative}\right)$$

where OD_{exper}, $OD_{negative}$, and $OD_{positive}$ represent the measured absorbance of the nanoparticle sample, negative control, and positive control, respectively.

Cytocompatibility Test of $_{h}CeO_2$@CA-074Me NPs with L929 Cells and MC3T3-E1 Cells

To assess the toxicity of the combined treatment with $_{h}CeO_2$@CA-074Me NPs, CCK8 was used to evaluate the cytotoxicity. L929 cells and MC3T3-E1 cells were seeded into 96-well plates at a density of 5×10^3 cells per well. The cells were treated with the $_{h}CeO_2$@CA-074Me NPs for 24, 48, and 72 h. After removal of the medium, the cells were washed three times with PBS, and the cells were added with 10% CCK8 reagent and incubated at 37°C in the dark for 1 h. The absorbance at 450 nm was measured using a microplate reader. To assess the effect of nanoparticles on absorbance at 450 nm, and the experiment was repeated three times.

Osteogenic Differentiation

MC3T3-E1 cells were seeded into six-well plates at 10×10^4 cells per well and divided into five groups: the first group was the blank control group. The second group was treated with *P.g*-LPS (1 μg/mL) for 4 h to establish an in vitro inflammation model. The third group was pretreated with *P.g*-LPS for 4 h and then treated with CA-074Me (100 μM) as a positive control group. Four to five groups were treated with *P.g*-LPS (1 μg/mL) for 4 h followed by the addition of safe concentrations of the groups of $_{h}CeO_2$ and $_{h}CeO_2$@CA-074Me NPs. MC3T3-E1 cells were cultured in a 6-well plate with growth medium. When the cells reached 80% confluence, they were cultured in osteogenic induction medium, which consisted of 10% FBS, 90% DMEM, 0.1 μM dexamethasone, 50 μM ascorbic acid-2-phosphate, and 10 mM β-glycerophosphate. The medium was replaced every three days. After 7, 14, and 21 d of induction, total RNA was extracted and quantitative real-time-polymerase chain reaction (RT-PCR) was performed to detect the expression of osteogenesis-related genes. The activity of alkaline phosphatase (ALP) was detected using an ALP kit (Jiancheng, Nanjing, China) and stained with a BCIP/NBT Alkaline Phosphatase Color Development Kit (Beyotime, Shanghai, China). After 21 d of induction, alizarin red S staining was used to evaluate cell mineralization in vitro (Beyotime, Shanghai, China). This process was repeated three times for each group of samples.

Real-Time PCR

Real-Time PCR of Inflammation

Cells were grouped and treated as RAW 264.7 cells were seeded into six-well plates at 3×10^4 cells per well and divided into five groups: the first group was the blank control group. The second group was treated with *P.g*-LPS (1 μg/mL) for 4 h to establish an in vitro inflammation model. The third group was pretreated with *P.g*-LPS for 4 h and then treated with CA-074Me (100 μM) for 24 h as a positive control group. Four to five groups were treated with *P.g*-LPS (1 μg/mL) for 4 h followed by the addition of safe concentrations of the groups of $_{h}CeO_2$ and $_{h}CeO_2$@CA-074Me NPs for 24 h. Then, the expressions of CTSB-NLRP3 pathway-related factors and macrophage phenotype were measured using quantitative real-time PCR. The total RNA of RAW264.7 cells was extracted using RNA-Easy (Vazyme). The

Table 1 Primer Sequences Used for RT-PCR

Gene	Forward Sequence (5′ to 3′)	Reserve Sequence (5′ to 3′)
β-Actin	CATCCGTAAAGACCTCTATGCCAAC	ATGGAGCCACCGATCCACA
OPG	GTGGAATAGATGTCACCCTGTGT	TTTGGTCCCAGGCAAACTGR
Runx-2	CCTCCAGCATCCCTTTCTT	CCTTTTCCCTCCTTGCCT
Col-1	GACATGTTCAGCTTTGTGGACCTC	GGGACCCTTAGGCCATTGTGTA
OPN	GCAGCTCAGAGGAGAAGAAGC	TTCTGTGGCGCAAGGAGATT
IL-1β	TCCAGGATGAGGACATGA GCAC	GAACGTCACACACCAGCAGGTTA
IL-6	CCACTTCACAAGTCGGAGGCTTA	CCAGTTTGGTAGCATCCATCATTTC
IL-10	ATGCTGCCTGCTCTTACTGACTG	CCCAAGTAACCCTTAAAGTCCTGC
Arg	CTCCAAGCCAAAGTCCTTAGAG	AGGAGCTGTCATTAGGGACATC
ASC	AGAGACATGGGCTTACAG GAGC	CCACAAAGTGTCCTGTTCT GC
Caspase-1	TGCCGTGGAGAGAAACAA GGA	TGGTGTTGAAGAGCAGAAA CA
TNF-α	ACTCCAGGCGGTGCCTA TGT	GTGAGGGTCTGGGCCAT AA
TGF-β	CTTCAGCCTCCACAGAGAA GAACT	TGTGTCCAGGCTCC AT A
CTSB	CTTCCCATGTCGGCAATCAG	GTGTAGTTGAGA GGTGGA
NLRP3	CCTGACCCAAACCCACCAGT	TTCTTTCGGA AGGCT TTA

RNA was reverse-transcribed into cDNA using a reverse transcription kit (ABScript III Master Mix for qPCR with gDNA Remover, ABclomal). Real-time PCR was performed using Universal SYBR Green Mix (ABclomal), cDNA, and primers under the following conditions: 95°C for 5 s and 60°C for 30s with 40 cycles. β-Actin served as an internal control for gene expression. Data results were analyzed with the $2^{-\Delta\Delta Ct}$ method. The primer sequences are shown in Table 1.

Real-Time PCR of Osteogenesis-Related Gene

MC3T3-E1 cells were seeded into six-well plates at density of 10×10^4 cells per well and divided into five groups, according to the method described in section Osteogenic Differentiation. When the cells reached 80% confluence, they were cultured in osteogenic induction medium containing 10% FBS, 90% DMEM, 0.1 μM dexamethasone, 50 μM ascorbic acid-2-phosphate, and 10 mM β-glycerophosphate) and the medium was changed every three days. After induction for 7, 14, and 21 d respectively, total RNA was extracted. To evaluate bone formation under inflammatory conditions, we measured the expression levels of osteogenesis-related genes (runt-related transcription factor 2 (Runx-2), collagen1 (Col-1), osteopontin (OPN), osteoprotegerin (OPG)) along with β-actin using real-time PCR.

Western Blot Assay

The cells were grouped and treated as in Section Real-time PCR of inflammation. After 24 h of treatment with nanoparticles, total proteins were extracted using RIPA buffer (Elabscience Biotechnology Co., Ltd). The proteins were separated using 10% gel (Epizyme, shanghai) and then transferred to PVDF membranes (Solarbio, Beijing). After blocking with fast blocking western (Solarbio, Beijing) for 10 min at room temperature, PVDF membranes were incubated with primary antibodies (CST, 1:1000) overnight at 4°C. β-Actin (Elabscience, 1:1000) was used as an internal reference. The membranes were then incubated with the secondary antibody HRP goat anti-rabbit IgG (Elabscience, 1:5000) for 1 h. Finally, each group of proteins was detected using electrochemiluminescent ECL reagents. The protein bands were quantified using Image software.

Statistical Analysis

All experiments were repeated three times, and data were analyzed using one-way ANOVA and Tukey's multiple-comparison test in GraphPad software, with a single asterisk indicating significant differences between data ($p< 0.05$) and two and more asterisks indicating a strong difference between data ($p< 0.005$). The data in the graphs represent mean ± standard deviation.

Results and Discussion

Characterization

The TEM images of $_{h}CeO_2$ and $_{h}CeO_2$@CA-074Me NPs are shown in Figure 1A and C. It can be seen from Figure 1A that $_{h}CeO_2$ NPs have a distinct hollow structure with a rough surface. Figure 1A and C also show that the addition of CA-074Me did not change the hollow morphology of $_{h}CeO_2$ NPs, with dispersed CA-074Me surrounding the $_{h}CeO_2$ particles. The DLS data (Figure 1B) indicates that the average particle size of $_{h}CeO_2$ NPs is approximately 97.34 nm and the standard deviation is 19.81 nm. The dynamic light scattering (DLS) data (Figure 1D) indicates that the average particle size of $_{h}CeO_2$@CA-074Me NPs is approximately 198.85 nm and the standard deviation is 28.39 nm. The zeta potentials for $_{h}CeO_2$ and $_{h}CeO_2$@CA-074Me NPs are measured at 12.74 mV and −1.54 mV respectively (Figure 1E), which suggest that $_{h}CeO_2$ and $_{h}CeO_2$@CA-074Me NPs lack stability and are prone to agglomeration. Zeta potential is closely related to dispersion stability, with larger absolute values indicating better dispersion stability. A zeta potential of less than ±10 mV is indicative of an unstable state, whereby particles exhibit minimal electrostatic repulsion and are highly susceptible to agglomeration or flocculation. This results in a tendency for particles to agglomerate or flocculate. The literature suggests that the small size and large specific surface area of nanoparticles contribute to their higher surface energy, and the occurrence of agglomeration is prone to happen. This trend becomes more evident as the size of nanoparticles in the 1–100 nm range decreases.[24] The smaller nanoparticle diameter in our experiment increases the surface area-to-volume ratio, which enhances the surface energy and makes the nanoparticles more prone to aggregation. As a result, the aggregation reduces the effective surface charge density, leading to a lower zeta potential measurement.

As shown in Figure 1F, the XRD test of the synthesized $_{h}CeO_2$ NPs is consistent with the typical cerium spectrum (JSPDS-34-0394), confirming its cubic fluorite structure. It is worth noting that the XRD test of $_{h}CeO_2$@CA-074Me NPs also matches the spectrum of $_{h}CeO_2$ NPs, indicating that CA-074Me is highly dispersed or doped into the lattice of $_{h}CeO_2$ NPs or its relative concentration mixed into the product is low. Figure 1G has three distinct characteristic peaks were observed at 1515, 1345, and 900 cm^{-1}. The background spectrum of $_{h}CeO_2$ NPs contains bands corresponding to surface hydroxyl groups. The absorbance peaks in the range of 900–400 cm^{-1} are attributed to Ce-O bonds and crystalline cerium oxide active phonon modes.[29] Additionally, cerium oxide typically contains carbonates, which are believed to be present in the subsurface layer and correspond to bands in the 1600–1260 cm^{-1} region.[30] In the physical mixture FTIR spectrum of $_{h}CeO_2$@CA-074Me NPs with the addition of CA-074Me, the stretching vibration band of GA at 1110^{-1} gradually weakens. These changes indicate strong molecular interactions between $_{h}CeO_2$ NPs and CA-074Me through self-assembly of polyelectrolyte complexes, including hydrogen bonding and electrostatic attraction. As shown

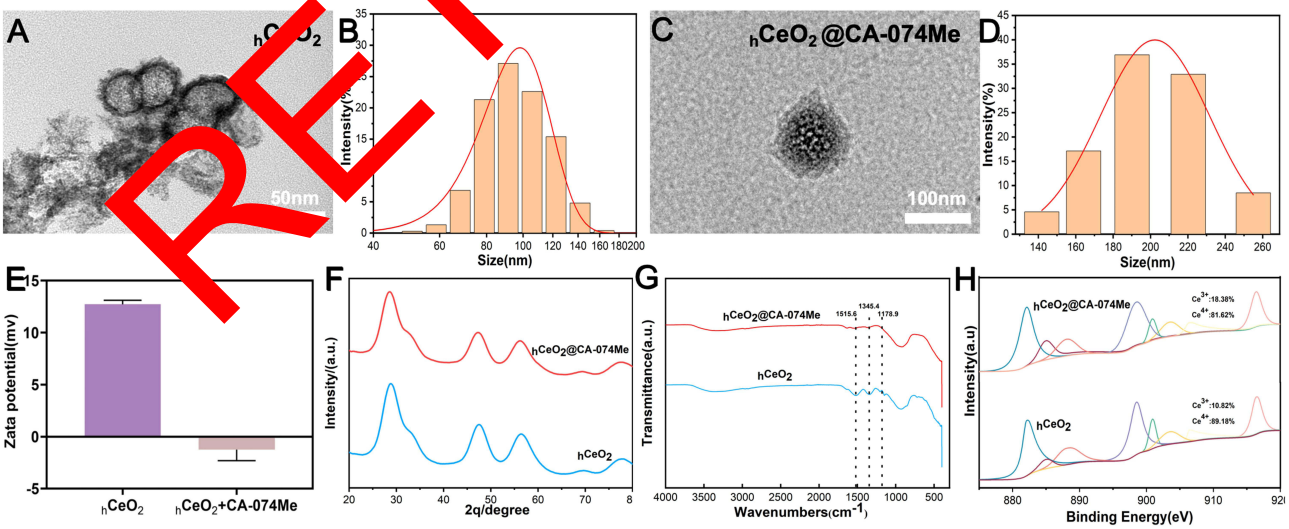

Figure 1 Characterization of $_{h}CeO_2$ and $_{h}CeO_2$@CA-074Me NPs. (**A**) TEM image of $_{h}CeO_2$ NPs. (**B**) Particle size distribution of $_{h}CeO_2$ NPs. (**C**) TEM image of $_{h}CeO_2$@CA-074Me NPs. (**D**) Particle size distribution of $_{h}CeO_2$@CA-074Me NPs. (**E**) Zeta potential analysis of $_{h}CeO_2$@CA-074Me NPs. (**F**) XRD analysis of $_{h}CeO_2$@CA-074Me NPs. (**G**) FTIR analysis of $_{h}CeO_2$@CA-074Me NPs. (**H**) XPS analysis of $_{h}CeO_2$@CA-074Me NPs.

in Figure 1H XPS analysis reveals peaks at 885.0 and 903.5 eV belonging to Ce^{3+} in $_hCeO_2$ NPs, along with peaks at the peaks at 882.1, 888.1, 898.5, 900.9, 906.4, and 916.4 eV were in Ce^{4+}, indicating its potential for mimicking peroxidase and superoxide dismutase activities and the coexistence of the two indicates that it has peroxidase-mimicking activity and superoxide dismutase mimetic activity potential. In addition, after quantitative calculations, the percentage of Ce^{3+} in $_hCeO_2$ NPs was 10.82%, and the percentages of Ce^{3+} in $_hCeO_2$@CA-074Me NPs, were 18.38%. The content of Ce^{3+} showed an increasing tendency with the increase of CA-074Me incorporation.

Evaluation of the Enzyme Mimetic Activity and ROS Scavenging Capacity of $_hCeO_2$@CA-074Me NPs

ROS are a natural by-product of cellular metabolism and include chemicals such as superoxide anion ($O_2^{-}\cdot$), hydroxyl radical (·OH), and hydrogen peroxide (H_2O_2). These chemicals play a crucial role in regulating various physiological functions in organisms and are involved in many biological processes.[31] The intrinsic biochemical properties of ROS form the basis of the necessary mechanisms for organismal development. However, excessive production of ROS can lead to oxidative stress, which is closely associated with macrophage polarization,[32] inflammation,[33] and bone diseases.[34] It is known that excessive ROS production can affect the differentiation of macrophages and drive them towards the M1 phenotype, resulting in the secretion of inflammatory cytokines, exacerbating local inflammation, and damaging tissues.[35] At the same time, chronic or long-term generation of ROS is at the core of the progression of inflammatory diseases.[36] Research has shown that ROS activate the NF-κB pathway. As an upstream signaling molecule, NF-κB pathway stimulates the release of CTSB and the activation of NLRP3 inflammasomes, promoting the aggregation of inflammatory cells and the expression of inflammatory factors.[37,38] The potential role of ROS in metabolic bone disease has received much attention.[28] Excessive and sustained levels of ROS can initiate mitochondrial apoptosis signaling, suppress the expression of bone formation markers, and attenuate osteogenic activity. Additionally, oxidative stress can induce the death of osteoblasts and bone cells while inhibiting the differentiation of osteogenic cells from bone marrow progenitor cells.[39] In conclusion, ROS plays a critical role in promoting inflammation by inducing oxidative stress, facilitating macrophage polarization toward the M1 phenotype, increasing lysosomal membrane permeability to promote CTSB release and activating NLRP3 inflammasomes. It also inhibits osteoblasts differentiation through oxidative stress. Therefore, scavenging ROS is essential to improve the inflammatory osteogenic microenvironment.

The most common antioxidant enzymes that help protect cells from the effects of free radicals are SOD, CAT, and glutathione peroxidase. These enzymes play a crucial role in the body's defense system by scavenging harmful free radicals and maintaining the redox balance of healthy cells. For example, CAT breaks down hydrogen peroxide into molecular oxygen and water, protecting cells from its toxicity. Similarly, SOD removes excess superoxide anion radicals, such as $O_2^{-}\cdot$, to prevent oxidative damage. In addition to these natural enzymes, CeO_2 NPs has been found to mimic the behavior of SOD and CAT by creating surface oxygen vacancies. This unique property allows CeO_2 NPs to effectively attenuate and eliminate the generation of ROS, making it a promising antioxidant biomaterial.[40–42] In recent years, there has been a growing interest in using CeO_2 NPs for the treatment of inflammation. Studies have shown that CeO_2 NPs can alleviate local inflammatory responses by scavenging excessive ROS and inhibiting the NF-κB pathway, which is responsible for regulating inflammation.[43–45] Meanwhile, CeO_2 NPs can eliminate ROS, promote cell proliferation, induce differentiation into osteogenic cells and protect osteogenic cells from damage.[46]

As shown in Figure 2A–C, the data clearly demonstrate that both $_hCeO_2$ and $_hCeO_2$@CA-074Me NPs exhibit enhanced SOD, CAT, and total antioxidant properties. Additionally, there is no statistically significant difference in their abilities when doped with CA-074Me. From the above discussion, it can be seen that $_hCeO_2$@CA-074Me NPs exhibited superior enzyme mimicry activity may due to the enhanced Ce^{3+}/Ce^{4+} ratio resulting from doping CA-074Me (Figure 1H). The antioxidant properties of $_hCeO_2$ and $_hCeO_2$@CA-074Me NPs were investigated during ROS scavenging. The ROS levels were confirmed using inverted fluorescence microscopy, as illustrated in Figure 2D. This revealed a reduction in the fluorescence intensity of both $_hCeO_2$ and $_hCeO_2$@CA-074Me NPs compared to the positive control group. Further analysis indicates that the conversion between Ce^{3+} and Ce^{4+} within $_hCeO_2$ NPs may contribute to this

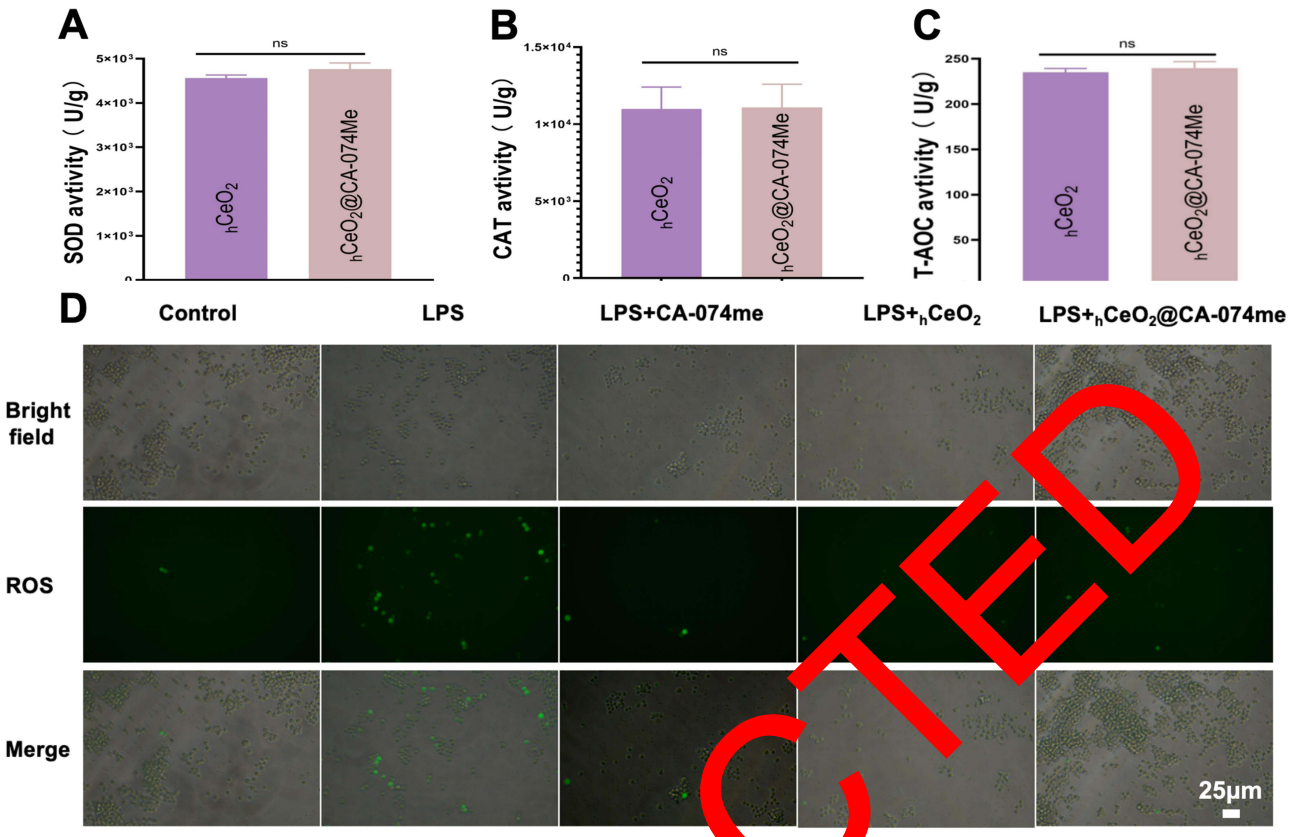

Figure 2 The enzyme simulated activity of $_hCeO_2$ and $_hCeO_2$@CA-074Me N[illegible] ability to s[illegible]ROS. (**A**) Superoxide dismutase (SOD) activity of $_hCeO_2$ and $_hCeO_2$@CA-074Me NPs. (**B**) Catalase (CAT) activity of $_hCeO_2$ and $_hCeO_2$@CA-074Me [illegible]. (**C**) Total antioxidant capacity (T-AOC) activity of $_hCeO_2$ and $_hCeO_2$@CA-074Me NPs. (**D**) Intracellular ROS levels in RAW 264.7 cells treated with *P.g*-LPS alone or co-[illegible]tion with $_hCeO_2$ and $_hCeO_2$@CA-074Me NPs. Scale bar: 25 μm.

phenomenon, as it enables effective elimination of ROS. The experimental results demonstrate that doped CA-074Me can also enhance the role of $_hCeO_2$ NPs in [illegible] in vitro.

Biocompatibility Assessment

Studies have shown that nanoparticles, especially metal-based nanoparticles, may induce various adverse reactions in cells, such as cell death. The experimental results obtained by MC3T3-E1 cells were consistent with those of L929 cells. Figure 3A and B indicate that $_hCeO_2$ NPs at concentrations ranging from 0 to 50 μg/mL show good cell compatibility at 24, 48, and 72 h without significant differences. However, at concentrations above 50 μg/mL, significant cytotoxicity is observed and increases with higher concentrations. Subsequently, this experiment detected the cytotoxicity of $_hCeO_2$@CA-074Me NPs, the results indicate that it exhibits good cell compatibility at 24, 48, and 72 h without significant differences (Figure 3B). In terms of blood compatibility, the hemolysis results (Figure 3C) show that the $_hCeO_2$ NPs have excellent blood compatibility. In summary, the nanoparticles synthesized in this study exhibit good biocompatibility at a concentration of 50 μg/mL, which is considered safe for subsequent experiments.

In other studies, doses exceeding 50 μg/mL have also been demonstrated to induce cytotoxicity. For example, Cheng et al observed that concentrations exceeding 50 μg/mL induced morphological damage, apoptosis and reduced viability in human hepatocellular carcinoma SMMC-7721 cells following incubation with hexahedral CeO_2 NPs concentrations ranging from 0 to 200 μg/mL for 24, 48, and 72 h.[48] Another study about the impact of three distinct CeO_2 NPs forms on HepG2 cells demonstrated that significant alterations in cellular morphology were evident at doses of 50 and 100 μg/mL.[49] These findings were corroborated by experimental data obtained in our laboratory. In conclusion, the $_hCeO_2$@CA-074Me NPs we synthesized have good biocompatibility at 50 μg/mL. In subsequent experiments, the safe concentration of the $_hCeO_2$@CA-074Me NPs is also set at 50 μg/mL.

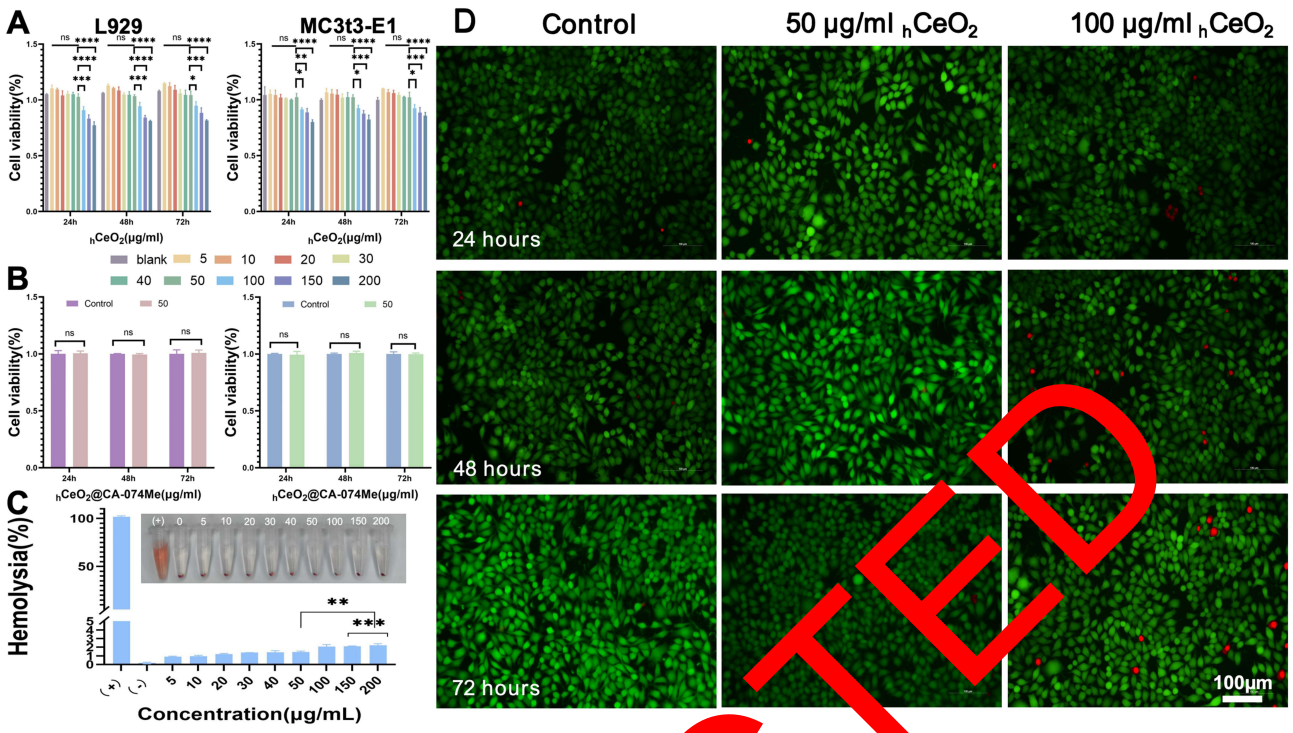

Figure 3 Biocompatibility of $_h$CeO$_2$ and $_h$CeO$_2$@CA-074Me NPs. (**A**) The 24, 48, and 72 h cytocompatibility of $_h$CeO$_2$ NPs respectively. (**B**) The 24, 48, and 72 h cytocompatibility of $_h$CeO$_2$@CA-074Me NPs respectively. (**C**) Blood compatibility of $_h$CeO$_2$@CA-074Me NPs. (+) and (-) represent positive and negative controls, respectively. (**D**) Live/dead fluorescence staining images of L929 treated with $_h$CeO$_2$ NPs for 24, 48, and 72 h. Scale bar: 100 μm. Data represent mean ± SD (n = 5; * represents significant differences. *p < 0.05, **P < 0.005, ***P < 0.0005, ****P < 0.0001).

There is a paucity of data concerning the long-term toxicity and ultimate fate of CeO_2 NPs employed in medical applications. This is likely attributable to the financial burden associated with maintaining animal models and the constrained scope for long-term monitoring of nanomaterials. The number of studies is insufficient to allow for any definitive conclusions to be drawn. One of the studies suggested that CeO_2 NPs do not exhibit toxicity in vitro nor in healthy rodents under standard therapeutic doses.[17] They remain in the liver for an extended period following administration, at least several months. Subsequently, CeO_2 NPs degrade into innocuous Ce^{3+}, which are expelled via the kidney. Additionally, it can be observed that CeO_2 NPs only exhibit toxicity in rodents when administered at high doses (>0.1 mg of CeO_2 per kg of animal), while they demonstrate hepatoprotective effects against various induced damages at doses up to 1 mg/kg body weight (bw). A comparable pattern is observed in vitro, where in CeO_2 NPs administered at elevated doses and also when they precipitate in the cell culture media, result in compromised cellular viability. Conversely, CeO$_2$ NPs typically demonstrate cytoprotective effects against a range of insults at doses spanning from 1 to 100 μg/mL. One of the most comprehensive studies was a two-year combined chronic toxicity study developed at BASF SE (Ludwigshafen, Germany). Carcinogenicity studies were conducted in accordance with the Organization for Economic Cooperation and Development (OECD) Test Guideline 453. The effects of CeO_2 NPs (40 nm), administered at doses of 0.1, 0.3, 1, and 3 mg m^{-3}, were evaluated following 3- or 6- months inhalation exposure to rats (5–7 weeks old female Wistar rats). The results demonstrated that CeO_2 NPs did not induce notable genotoxicity in the alkaline comet assay and micronucleus test.[27] Consequently, the biokinetics of CeO_2 NPs is contingent upon their intrinsic characteristics, their evolution within the physiological milieu, the dosage employed, and the route of exposure.

Toxicological studies have revealed a variety of potential effects of CeO_2 NPs, including pulmonary inflammation, cytotoxicity, genotoxicity, hepatotoxicity, and neurotoxicity. However, these effects have not yet been fully characterized. Epidemiological studies have demonstrated that CeO_2 NPs have deleterious effects on the respiratory tract, including sensory irritation and airflow limitation. It is therefore recommended that further in-depth studies be conducted in order to establish a safe therapeutic window for the drug, prior to incorporating CeO_2 NPs into therapeutic regimens for human

https://doi.org/10.2147/IJN.S389156

diseases. It is anticipated that CeO_2 NPs will become a subject of growing interest in future research. In order to identify the CeO_2 NPs most suitable for human applications, it will be necessary for researchers to study the pathology and toxicology of CeO_2 NPs from the perspective of pathogenesis.

$_h$CeO$_2$@CA-074Me NPs Could Inhibit Inflammation and Improve the Osteogenic Inflammatory Microenvironment

Promote Macrophage Polarization from M1 Phenotype to M2 Phenotype

Nanoparticles with different physicochemical properties (such as chemical composition, size and surface modification) have been shown to induce macrophage polarization.[50,51] Therefore, macrophages serve as a target for nanoparticle therapy and can be regulated in the treatment of inflammation-related diseases by differentiating into anti-inflammatory phenotype. ROS play a pivotal role in macrophage-mediated inflammation. Studies have shown that ROS serve as the primary driving signal for the activation of M1 polarization in macrophage. If excessive ROS stimulation led to prolonged activation of M1 macrophage, a significant number of inflammatory factors will be released, creating a chronic inflammatory environment and disrupting bone homeostasis. This disruption of the balance between antioxidants and ROS can result in heightened oxidative stress in local tissues, leading to a shift in macrophage polarization from M2 to M1. This shift can impede the osteogenic differentiation of endogenous stem cells.[52] Additionally, ROS have been found to have direct effects on osteogenesis. Increased levels of endogenous ROS induced by LPS can upregulate the expression of inflammatory cytokines, and ROS is a major type of free radical involved in bone remodeling and destruction. ROS also inhibit the expression of Runx2 and Osterix, reducing osteogenic activity. Furthermore, following ROS induction, the expression of osteoclasts markers such as c-fos, NFATc1, and TRAP increases. Therefore, the elevated levels of ROS and the shift towards M1 phenotype macrophage have a deleterious impact on the bone formation microenvironment.

In our experiments, the mRNA expression of polarization markers IL-6, IL-1β, and TNF-α in M1 phenotype macrophage decreased upon addition of $_h$CeO$_2$@CA-074Me NPs (Figure 4A and B). These pro-inflammatory mediators have the ability to induce local or systemic inflammation. On the other hand, the mRNA expression of polarization markers Arg, IL-10, and TGF-β in M2 phenotype macrophage significantly increased with statistical significance

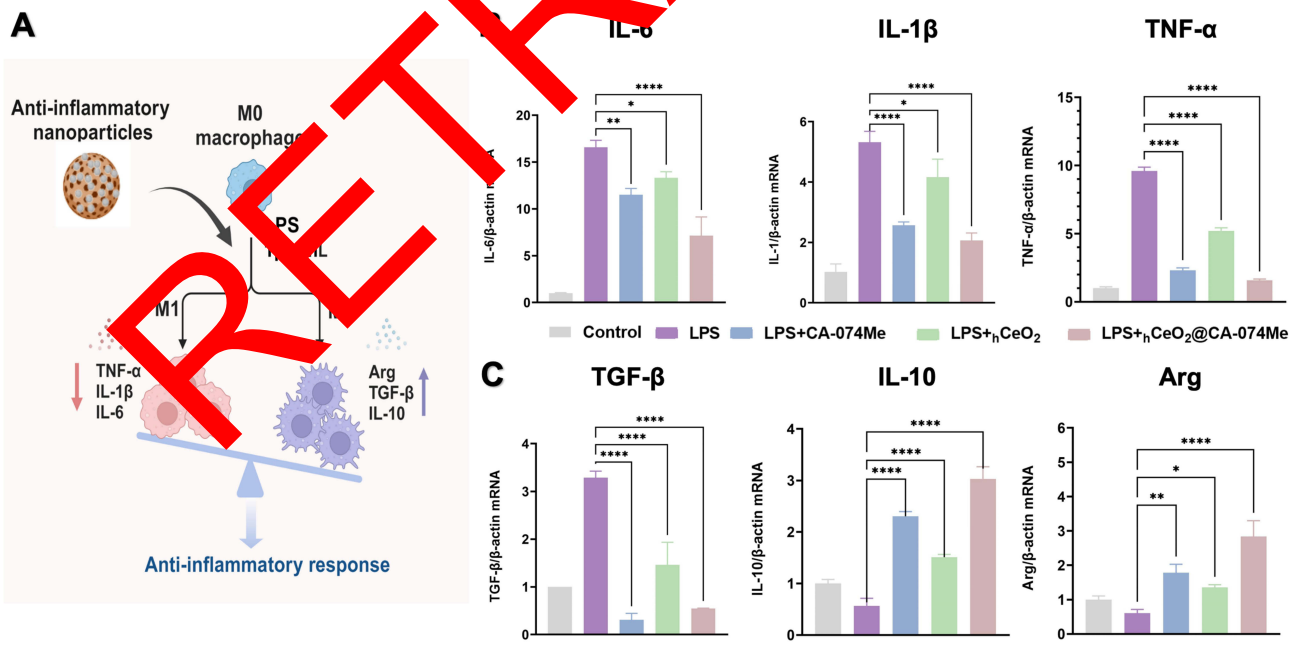

Figure 4 The effect of $_h$CeO$_2$@CA-074Me NPs on the polarization phenotype of macrophages. (**A**) The schematic diagram of $_h$CeO$_2$@CA-074Me NPs on the polarization phenotype of macrophages. (**B**) The mRNA expression of IL-6, TNF-α and IL-1β that polarizing markers of M1 phenotype macrophage. (**C**) The mRNA expression of IL-10, Arg, and TGF-β that polarizing markers of M2 phenotype macrophage. (n=3; * represent significant differences. *P < 0.05, **P < 0.005, ****P < 0.0001).

(Figure 4C). These findings indicate that $_{h}CeO_2$@CA-074Me NPs can modulate the immune microenvironment by promoting macrophage polarization from the pro-inflammatory M1 phenotype to the anti-inflammatory M2 phenotype.

Studies have shown that CeO_2 NPs with a higher Ce^{4+}/Ce^{3+} ratio, deposited on titanium substrates by magnetron sputtering and vacuum annealing, increase polarization towards the M2 phenotype in mouse macrophages.[21] Additionally, research has demonstrated that coating implant surfaces with CeO_2 NPs with a high Ce^{4+}/Ce^{3+} ratio can reduce M1 macrophages polarization and suppress inflammation, while promoting active M2 macrophages to regulate periodontal tissue regeneration.[53] Furthermore, previous literature suggested that CA-074Me can reduce lipid peroxidation and mitochondrial dysfunction in macrophages, leading to M2 macrophage polarization.[54] The significant inhibitory effect of $_{h}CeO_2$@CA-074Me NPs on the expression of M1 markers can be attributed to the predominant simulating activity of SOD and CAT, which effectively eliminates ROS generated by LPS stimulation. This mechanism plays a crucial role in the nanoparticles' antioxidant and anti-inflammatory effects.

$_{h}CeO_2$@CA-074Me NPs Could Inhibit the CTSB-NLRP3 Signaling Pathway to Rectify the Inflammatory Osteogenic Environment

As illustrated in Figure 5A–C, the results of RT-PCR and Western blot analysis revealed a significant increase in CTSB levels following LPS stimulation. However, co-culturing with $_{h}CeO_2$ NPs, CA-074Me, or $_{h}CeO_2$@CA-074Me NPs resulted in a significant decrease observed with $_{h}CeO_2$@CA-074Me NPs. Figure 5C further demonstrates that LPS treatment led to an increase in NLRP3, ASC, and caspase-1 expression, which was subsequently reduced upon addition of CA-074Me. This suggests that the decrease in CTSB levels resulted in a decrease in NLRP3 inflammasome expression. The addition of nanomaterials also inhibited the assembly of NLRP3 inflammasome components, indicating that nanomaterials can reduce NLRP3 inflammasome expression by inhibiting CTSB anfd subsequently decreasing the release of inflammatory factors, thereby reducing the inflammatory response. The most significant reduction in this trend was observed with $_{h}CeO_2$@CA-074Me NPs, highlighting its superior anti-inflammatory effect. Upon activation of the NLRP3 inflammasome, pro-IL-18, and pro-IL-1β are cleaved into mature IL-18 and IL-1β.[55] As depicted in Figure 5C, the mRNA expression levels of inflammatory factors IL-18 and IL-1β were

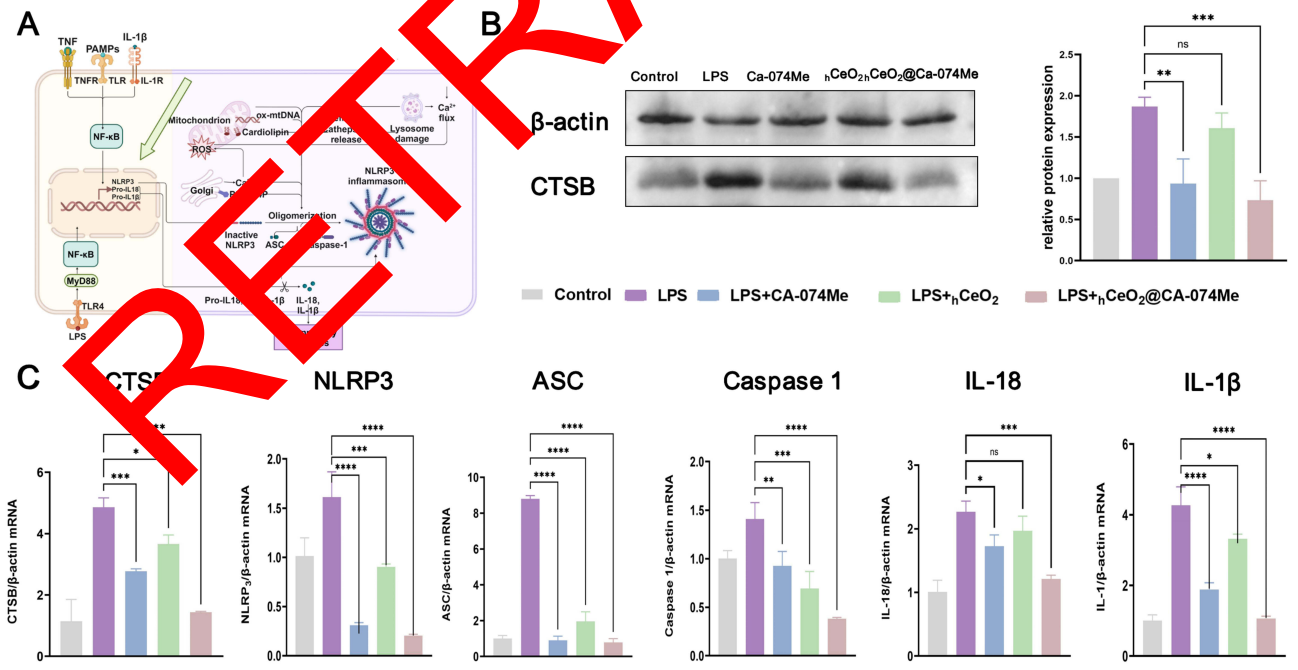

Figure 5 $_{h}CeO_2$@CA-074Me NPs could Inhibit the CTSB–NLRP3 signaling pathway in a *P.g*-LPS stimulated inflammation model in RAW264.7 cells. (**A**) The schematic diagram of $_{h}CeO_2$@CA-074Me NPs on the CTSB-NLRP3 signaling pathway. (**B**) Western blot analysis of CTSB protein expression upon RAW264.7 cells treated with 1 μg/mL *P.g*-LPS for 4 h and $_{h}CeO_2$@CA-074Me NPs for 24 h. (**C**)The mRNA expression of CTSB, NLRP3, ASC, Caspase 1, IL-18 and IL-1β in RAW264.7 cells treated with *P. g*-LPS for 4 h and $_{h}CeO_2$@CA-074Me NPs for 24 h. (n = 3; * represent significant differences. *P < 0.05, **P < 0.005, ***P < 0.0005, ****P < 0.0001.).

https://doi.org/10.2147/IJN.S389156

increased in the LPS-treated group, but decreased upon addition of CA-074Me. These results demonstrate the involvement of CTSB in the LPS-induced inflammatory response. Furthermore, the addition of $_{h}CeO_2$@CA-074Me NPs resulted in a decrease in CTSB, IL-18, and IL-1β expression levels, indicating its ability to alleviate inflammation by inhibiting CTSB.

The dual-signaling model is currently the most widely accepted hypothesis in the field. Firstly, LPS or other microbial molecules, as previously described, act as an initial signal to upregulate the expression of NLRP3. The second signal can enable the activation of NLRP3 by a number of different stimuli, including ATP, ROS, and CTSB. Of these, CTSB, a lysosomal enzyme that is widely expressed in mammalian cells, serves as a marker for lysosomal damage.[56] It is noteworthy that an increase in ROS and CTSB has been observed in the context of inflammatory conditions, which can further exacerbate the activation of NLRP3 and serve to exacerbate the inflammatory environment, ultimately resulting in apoptosis.[57] The NLRP3 inflammasome can be activated by a variety of stimuli, resulting in the oligomerization of apoptosis-associated speck-like protein containing a CARD (ASC) and the recruitment of pro-caspase-1 for maturation and release of IL-1β. This release of IL-1β is a marker for M1-like macrophage polarization.[58] Macrophages play an active role in bone physiology and pathology, producing cytokines that exert a substantial regulatory influence on osteogenesis.[59] Concurrently, studies have demonstrated that the inhibition of NLRP3 inflammasome activation can markedly influence macrophage plasticity, thereby regulating chronic inflammation, enhancing osteogenic function, and facilitating bone formation within the body.[2] To gain further insight into the impact of nanoparticles on the CSTB-NLRP3 signaling pathway, cells were treated with nanoparticles for 24 h. The results demonstrated that $_{h}CeO_2$ NPs, CA-074Me, and $_{h}CeO_2$@CA-074Me NPs exhibited notable inhibitory effects on gene expression associated with the NLRP3 inflammasome. Among these treatments, $_{h}CeO_2$@CA-074Me NPs exhibited the most pronounced effect. Potential explanations for this phenomenon are as follows: (1) An increase in ROS can facilitate lysosomal membrane permeabilization (LMP), resulting in the excessive release of CTSB. Nevertheless, $_{h}CeO_2$ @ CA-074Me NPs are capable of reducing Ce^{4+} to Ce^{3+}, thereby enabling them to clear ROS and, consequently, inhibiting the release of CTSB. (2) CA-074Me has been demonstrated to exert a direct and specific inhibitory effect on CTSB. Consequently, this dual mechanism effectively suppresses NLRP3 activation and mitigates inflammation.

$_{h}CeO_2$@CA-074Me NPs Have the Potential of Osteogenesis Under Inflammatory Conditions

The results of the study showed that incorporating nanoparticles greatly improved the ability of MC3T3-E1 cells to produce bone tissue after being stimulated with *P.g*-LPS (1μg/mL) for 4 h. Specifically, when co-cultured with $_{h}CeO_2$@CA-074Me NPs, there was a significant increase in alkaline phosphatase expression, as shown by ALP staining (Figure 6A–C). This was supported by quantitative ALP analysis (Figure 6B) and alizarin red staining, which demonstrated increased calcium deposition in MC3T3-E1 cells (Figure 6D). These findings suggest that $_{h}CeO_2$@CA-074Me NPs is an effective agent for promoting bone formation in an inflammatory environment.

Many signaling molecules and transcription factors are involved in the growth and differentiation of osteoblasts. The expression profiles of these osteogenic genes were examined in Figure 7A–C after treating MC3T3-E1 cells with LPS as a positive control and co-culturing them with $_{h}CeO_2$ NPs, CA-074Me, and $_{h}CeO_2$@CA-074Me NPs for 7, 14, and 21 d, respectively. The levels of OPN, OPG, and Col-1 were significantly higher in the $_{h}CeO_2$@CA-074Me NPs group compared to the $_{h}CeO_2$ NPs or CA-074Me groups at days 7, 14, and 21. Study has demonstrated that LPS stimulation can effectively enhance the osteogenic differentiation of EMSCs.[60] In our experimental results, the osteogenic effect observed in the MC3T3-E1 cells group treated with LPS alone was more pronounced than that of the control group. This effect may be attributed to inflammatory adaptive mechanisms that enhance the paracrine capacity of MC3T3-E1 cells.

Inflammation is a defensive response to external and/or internal signals, where inflammatory mediators such as ROS, pro-inflammatory cytokines, and chemokines directly or indirectly regulate the osteogenic microenvironment.[61] The macrophage is the main cellular mediator of cytokine production in bone metabolism and can switch between M1 (inflammatory) and M2 (repair) phenotype in response to environmental stimuli.[62] This behavior enables the accumulation of a greater number of anti-inflammatory macrophages during the initial phases of bone defect repair. This

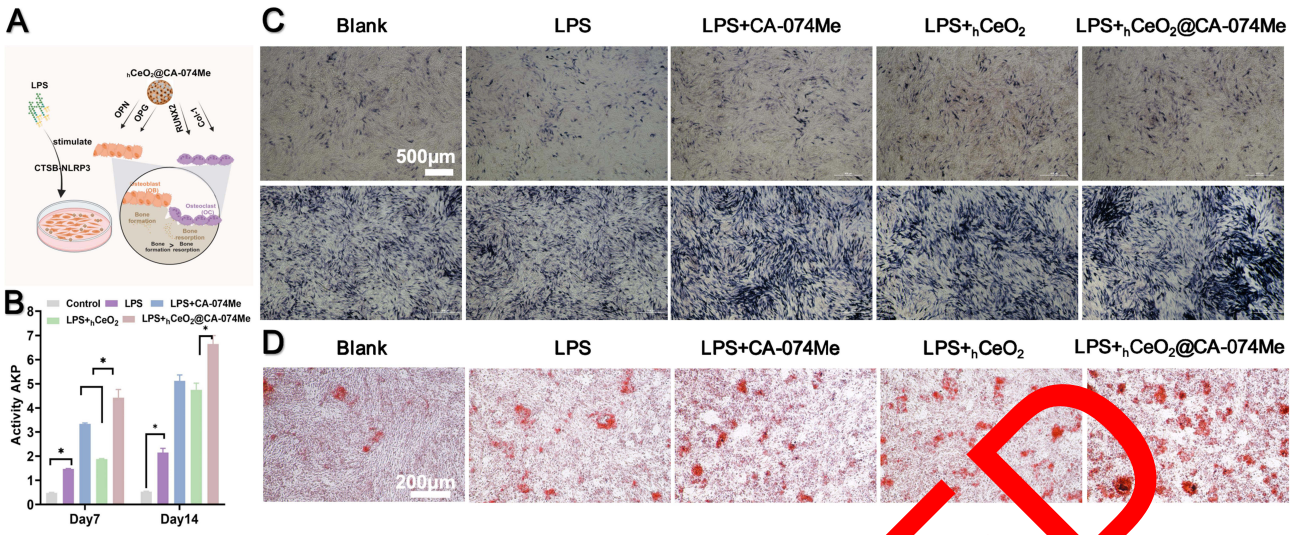

Figure 6 Osteogenic differentiation properties of MC3T3-E1 cells in a *P.g*-LPS stimulated inflammation model: (**A**) The illustration of the gene expression on $_{h}CeO_2$@CA-074Me NPs. (**B**) ALP staining images at 7 and 14 d. (**C**) ALP activity of cells cultured for 7 and 14 d. (**D**) ARS staining images at 21 d. The asterisks indicate a statistically significant difference from the groups (n = 3; * represent significant differences. *p < 0.05).

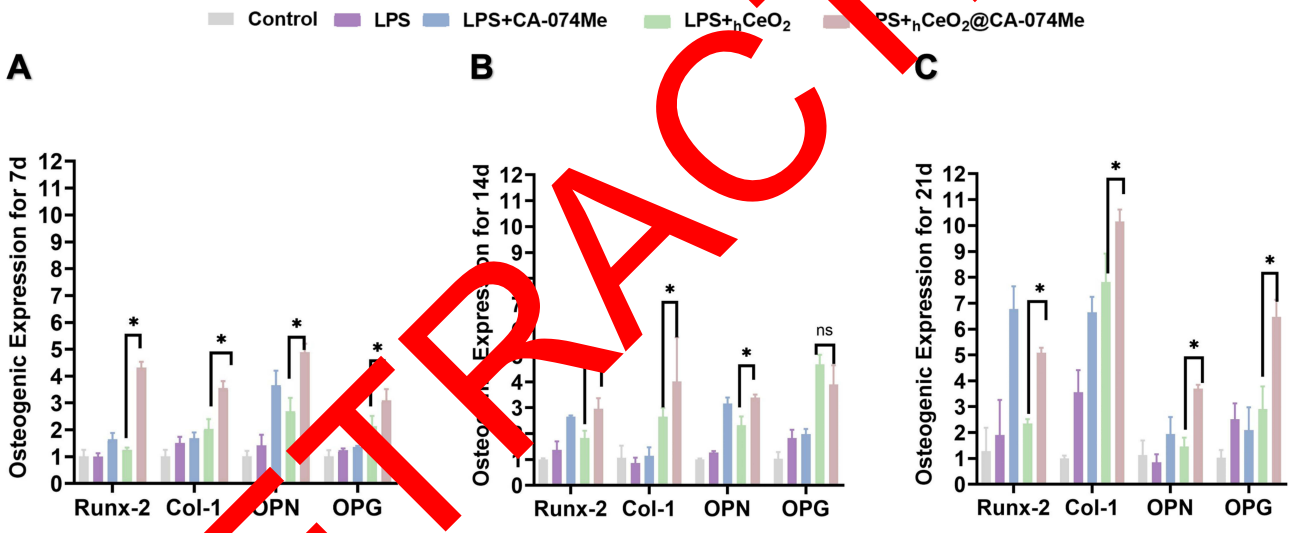

Figure 7 Osteogenic gene expression of MC3T3-E1 cells in a *P.g*-LPS stimulated inflammation model: (**A**) relative osteogenic gene expression of cells after culturing for 7 d. (**B**) relative osteogenic gene expression of cells after culturing for 14 d. (**C**) relative osteogenic gene expression of cells after culturing for 21 d. Notes: Runt-related transcription factor 2 (Runx-2), collagen type I (Col-1), osteopontin (OPN), osteoprotegerin (OPG). The asterisks indicate a statistically significant difference from the groups (n = 3; * represent significant differences. *p < 0.05).

coordinated regulation of the immune microenvironment facilitates the mitigation of excessive inflammation and its detrimental effects.[63,64] Evidence suggested that osteoporotic mice have an elevated ratio of M1/M2 macrophages in their bone marrow, indicating a potential link between this ratio and bone loss. Therefore, targeting this ratio may be a potential therapeutic approach for osteoporosis.[65] Increased inflammation leads to higher levels of pro-inflammatory mediators, such as cytokines and chemokines, which negatively affect the function of bone cells and create an unfavorable microenvironment for osteoblasts. Studies have shown that TNF-α and IL-1β can downregulate the expression of OPG, inhibiting bone remodeling. Additionally, IL-1β can impede the activation of Runx2, hindering osteogenesis and osteoblast differentiation.[66] The NLRP3 inflammasome, when abnormally activated, plays a significant role in the pathogenesis of osteoporosis. It activates caspase-1, leading to the conversion of pro-IL-1β and pro-IL-18 into their mature forms, and upregulates bone resorption, hindering bone tissue generation.[67] Concurrently, the NLRP3

https://doi.org/10.2147/IJN.S389156

inflammasome can stimulate the production of pro-inflammatory cytokines, such as IL-1β and IL-18.[68] The compound $_{h}CeO_2$@CA-074Me NPs can reduce the release of CTSB, alleviate ROS, and inhibit the activation of the NLRP3 inflammasome. This promotes the polarization of macrophages from the M1 phenotype to the M2 phenotype, creating a more favorable environment for osteogenesis under inflammatory conditions.

Conclusion

In this study, a novel hybrid material, $_{h}CeO_2$@CA-074Me NPs, was developed by incorporating CA-074Me into $_{h}CeO_2$ NPs. This material demonstrates the ability to simultaneously promote osteogenesis while improving the inflammatory microenvironment. Specifically, $_{h}CeO_2$@CA-074Me NPs were found to regulate inflammation through a potential molecular mechanism primarily mediated by the inhibition of the CTSB-NLRP3 signaling pathway, which reduces inflammation. Additionally, $_{h}CeO_2$@CA-074Me NPs could facilitate the polarization of macrophages from the pro-inflammatory M1 phenotype to the anti-inflammatory M2 phenotype, reversing the inflammatory microenvironment by suppressing pro-inflammatory factor secretion and enhancing anti-inflammatory factor expression. By addressing both inflammation and osteogenesis, this material effectively improves bone formation in inflammatory conditions. This study offers a unique perspective on the potential to enhance the osteogenic microenvironment in inflammatory states, ultimately contributing to improved bone regeneration. The long-term toxicity of $_{h}CeO_2$ NPs cannot be fully determined at present in the absence of animal experiments, but based on the available in vitro data and theoretical analyses, the risk of toxicity may be closely related to the dose, particle properties and exposure time. Under reasonable dose control, $_{h}CeO_2$@CA-074Me NPs may exhibit high biocompatibility. However, their long-term safety must be thoroughly evaluated through subsequent experiments to ensure their potential benefits can be realized safely for use.

Ethics Approval and Informed Consent

The hemolysis experiments were performed using three 6-week-old male BALB/c mice approved by the Institutional Animal Ethics Committee of Qingdao University Laboratory Animal Centre (20231118BALB/C0320231126090) and in strict accordance with the Guidelines for Ethical Review of Welfare of Laboratory Animals in China (GB/T35892-2018).

Author Contributions

All authors made substantial contributions to the design and conception of the study and acquisition, analysis, and interpretation of data and took part in either drafting or revising the manuscript. All authors gave final approval for the version to be published, have agreed on the journal to which the article has been submitted, and agreed to be accountable for all aspects of the work in ensuring that questions related to the accuracy or integrity of any part of the work are appropriately investigated and resolved.

Funding

The author(s) declare that financial support was received for the research, authorship, and/or publication of this article. This work was supported by China Postdoctoral Science Foundation (2023M732676), Shandong Provincial Natural Science Foundation (ZR2021QH251 and ZR2024MH308), and Clinical Medicine +X Research Project of Affiliated Hospital of Qingdao University (QDFY+X2021055).

Disclosure

The authors declare that they have no competing interests in this work.

References

1. Wei F, Xiao Y. Modulation of the osteoimmune environment in the development of biomaterials for osteogenesis. *Adv Exp Med Biol*. 2018;1077:69–86.

2. Chen Y, Wu Y, Guo L, et al. Exosomal Lnc NEAT1 from endothelial cells promote bone regeneration by regulating macrophage polarization via DDX3X/NLRP3 axis. *J Nanobiotechnol*. 2023;21(1):98. doi:10.1186/s12951-023-01855-w
3. Sadowska JM, Ginebra MP. Inflammation and biomaterials: role of the immune response in bone regeneration by inorganic scaffolds. *J Mat Chem B*. 2020;8(41):9404–9427. doi:10.1039/D0TB01379J
4. Zhang H, Yuan Y, Xue H, et al. Reprogramming mitochondrial metabolism of macrophages by miRNA-released microporous coatings to prevent peri-implantitis. *J Nanobiotechnol*. 2023;21(1):485. doi:10.1186/s12951-023-02244-z
5. Yu T, Zhao L, Huang X, et al. Enhanced activity of the macrophage M1/M2 phenotypes and phenotypic switch to M1 in periodontal infection. *J Periodontol*. 2016;87(9):1092–1102. doi:10.1902/jop.2016.160081
6. Alam MI, Mae M, Farhana F, et al. NLRP3 inflammasome negatively regulates RANKL-induced osteoclastogenesis of mouse bone marrow macrophages but positively regulates it in the presence of lipopolysaccharides. *Int J Mol Sci*. 2022;23(11):6096. doi:10.3390/ijms23116096
7. Lundahl MLE, Mitermite M, Ryan DG, et al. Macrophage innate training induced by IL-4 and IL-13 activation enhances OXPHOS driven anti-mycobacterial responses. *eLife*. 2022;11.
8. Zhu K, Yang C, Dai H, et al. Crocin inhibits titanium particle-induced inflammation and promotes osteogenesis by regulating macrophage polarization. *Int Immunopharmacol*. 2019;76:105865. doi:10.1016/j.intimp.2019.105865
9. Wang J, Wang L, Zhang X, et al. Cathepsin B aggravates acute pancreatitis by activating the NLRP3 inflammasome and promoting the caspase-1-induced pyroptosis. *Int Immunopharmacol*. 2021;94:107496. doi:10.1016/j.intimp.2021.107496
10. Cavallo-Medved D, Sloane BF. Cell-surface cathepsin B: understanding its functional significance. *Curr Top Dev Biol*. 20[illegible]:54:313–341.
11. Gray AW, Davies ME, Jeffcott LB. Localisation and activity of cathepsins K and B in equine osteoclast[illegible] *Res Vet Sci*. 2[illegible]02;72(2):95–103. doi:10.1053/rvsc.2001.0522
12. Hsing LC, Kirk EA, McMillen TS, et al. Roles for cathepsins S, L, and B in insulitis and diabetes in the NOD mouse. *J Autoimmun*. 2010;34(2):96–104. doi:10.1016/j.jaut.2009.07.003
13. Baici A, Hörler D, Lang A, Merlin C, Kissling R. Cathepsin B in osteoarthritis: zonal variation of enzyme activity in human femoral head cartilage. *Ann Rheumatic Dis*. 1995;54(4):281–288. doi:10.1136/ard.54.4.281
14. Li X, Ji L, Men X, et al. Pyroptosis in bone loss. *Apoptosis*. 2023;28(3–4):293–312. doi:10.1007/s104[illegible]022-01[illegible]07-z
15. Kelley N, Jeltema D, Duan Y, He Y. The NLRP3 inflammasome: an overview of mechanisms of activation and regulation. *Int J Mol Sci*. 2019;20(13):3328. doi:10.3390/ijms20133328
16. Liang DYT, Wang YN, Qian K. Nanozymes: applications in clinical biomarker detection. *Interdiscip Med*. 2023;1(4). doi:10.1002/INMD.20230020
17. Casals E, Zeng M, Parra-Robert M, et al. Cerium oxide nanoparticles: advances in biodistribution, toxicity, and preclinical exploration. *Small*. 2020;16(20):e1907322. doi:10.1002/smll.201907322
18. Shlapa Y, Solopan S, Sarnatskaya V, et al. Cerium dioxide nanoparticles synthesized via precipitation at constant pH: synthesis, physical-chemical and antioxidant properties. *Colloids Surf B*. 2022;220:112960. doi:10.10[illegible]j.colsurfb.202[illegible]112960
19. Gupta A, Das S, Neal CJ, Seal S. Controlling the surface chemistry of cerium oxide nanoparticles for biological applications. *J Mat Chem B*. 2016;4(19):3195–3202. doi:10.1039/C6TB00396F
20. Chen BH, Stephen Inbaraj B. Various physicochemical and surface properties controlling the bioactivity of cerium oxide nanoparticles. *Crit Rev Biotechnol*. 2018;38(7):1003–1024. doi:10.1080/07388551.201[illegible]14265
21. Li J, Wen J, Li B, et al. Valence state manipulation of cerium oxide nanoparticles on a titanium surface for modulating cell fate and bone formation. *Adv Sci*. 2018;5(2):1700678. doi:10.1002/advs.2[illegible]700
22. Xiang J, Li J, He J, et al. Cerium oxide nanoparticle modified scaffold interface enhances vascularization of bone grafts by activating calcium channel of mesenchymal stem cells. *ACS Appl Mater Interfaces*. 2016;8(7):4489–4499. doi:10.1021/acsami.6b00158
23. Naidi SN, Harunsani MH, Tan AL, Khan [illegible]. Green-synthesized CeO(2) nanoparticles for photocatalytic, antimicrobial, antioxidant and cytotoxicity activities. *J Mat Chem*[illegible] 2021;9(28):[illegible]599–5620. doi:10.1039/D1TB00248A
24. Starsich FHL, Herrmann IK, Pra[illegible]SE. Nanoparticles for biomedicine: coagulation during synthesis and applications. *Annu RevChem Biomol Eng*. 2019;10:155–174. doi:10.[illegible]146/an[illegible]ev-chembioeng-060718-030203
25. Meng Z, Gao M, Wang C[illegible]uan S, Zhang[illegible]Lu J. Apigenin alleviated high-fat-diet-induced hepatic pyroptosis by mitophagy-ROS-CTSB-NLRP3 pathway in mice and AML12 cells. *J Agri Food Chem*. 2023;71(18):7032–7045. doi:10.1021/acs.jafc.2c07581
26. Gao Z, Luo K, Hu Y[illegible]t al. Melatonin alleviates chronic stress-induced hippocampal microglia pyroptosis and subsequent depression-like behaviors by inhibiting cathepsin B/NLRP3 signaling pathway in rats. *Transl Psychiatry*. 2024;14(1):166. doi:10.1038/s41398-024-02887-y
27. Wu J, Han Y, Xu H, e[illegible]ficient chaperone-mediated autophagy facilitates LPS-induced microglial activation via regulation of the p300/NF-κB/NLRP3 pat[illegible]*Sci Adv*[illegible]2023;9(4[illegible]eadi8343. doi:10.1126/sciadv.adi8343
28. Li F, Li[illegible]Song X[illegible]et al. Alginate/gelatin hydrogel scaffold containing nCeO(2) as a potential osteogenic nanomaterial for bone tissue engineering. *Int j[illegible]nomed*. 2[illegible]22;17:6561–[illegible]578. doi:10.2147/IJN.S388942
29. Elkho[illegible]hany[illegible], Ki[illegible]A, Kabary MA. Thermal, FTIR and UV spectral studies on tellurite glasses doped with cerium oxide. *Ceram Int*. 2018;44([illegible]89–2796. doi:10.1016/j.ceramint.2017.11.019
30. Mihaylov M[illegible]Ivanova EZ, Vayssilov GN, Hadjiivanov KI. Revisiting ceria-NOx interaction: FTIR studies. *Catal Today*. 2020;357:613–620. doi:10.1016/j.ce[illegible]d.2019.05.014
31. Nathan C, Cunningham-Bussel A. Beyond oxidative stress: an immunologist's guide to reactive oxygen species. *Nat Rev Immunol*. 2013;13(5):349–361. doi:10.1038/nri3423
32. Liu C, Hu F, Jiao G, et al. Dental pulp stem cell-derived exosomes suppress M1 macrophage polarization through the ROS-MAPK-NFκB P65 signaling pathway after spinal cord injury. *J Nanobiotechnol*. 2022;20(1):65. doi:10.1186/s12951-022-01273-4
33. Fraisl P, Aragonés J, Carmeliet P. Inhibition of oxygen sensors as a therapeutic strategy for ischaemic and inflammatory disease. *Nat Rev Drug Discov*. 2009;8(2):139–152. doi:10.1038/nrd2761
34. Seminko V, Maksimchuk P, Grygorova G, et al. Mechanism and dynamics of fast redox cycling in cerium oxide nanoparticles at high oxidant concentration. *J Phys Chem C*. 2021;125(8):4743–4749. doi:10.1021/acs.jpcc.1c00382
35. Kim J, Kim HY, Song SY, et al. Synergistic oxygen generation and reactive oxygen species scavenging by manganese ferrite/ceria co-decorated nanoparticles for rheumatoid arthritis treatment. *ACS nano*. 2019;13(3):3206–3217. doi:10.1021/acsnano.8b08785

36. Griffith B, Pendyala S, Hecker L, Lee PJ, Natarajan V, Thannickal VJ. NOX enzymes and pulmonary disease. *Antioxid Redox Signal*. 2009;11(10):2505–2516. doi:10.1089/ars.2009.2599
37. Morgan MJ, Liu ZG. Crosstalk of reactive oxygen species and NF-κB signaling. *Cell Res*. 2011;21(1):103–115. doi:10.1038/cr.2010.178
38. Codolo G, Plotegher N, Pozzobon T, et al. Triggering of inflammasome by aggregated α-synuclein, an inflammatory response in synucleinopathies. *PLoS One*. 2013;8(1):e55375. doi:10.1371/journal.pone.0055375
39. Zhang C, Li H, Li J, Hu J, Yang K, Tao L. Oxidative stress: a common pathological state in a high-risk population for osteoporosis. *Biomed Pharmacother*. 2023;163:114834.
40. Li X, Han Z, Wang T, et al. Cerium oxide nanoparticles with antioxidative neurorestoration for ischemic stroke. *Biomaterials*. 2022;291:121904. doi:10.1016/j.biomaterials.2022.121904
41. Heckert EG, Karakoti AS, Seal S, Self WT. The role of cerium redox state in the SOD mimetic activity of nanoceria. *Biomaterials*. 2008;29(18):2705–2709. doi:10.1016/j.biomaterials.2008.03.014
42. Dutta D, Mukherjee R, Ghosh S, Patra M, Mukherjee M, Basu T. Cerium oxide nanoparticles as antioxidant or pro-oxidant agents. *ACS Appl Nano Mater*. 2022;5(1):1690–1701. doi:10.1021/acsanm.1c04518
43. Sun Y, Sun X, Li X, et al. A versatile nanocomposite based on nanoceria for antibacterial enhancement and protection from aPDT-aggravated inflammation via modulation of macrophage polarization. *Biomaterials*. 2021;268:120614. doi:10.1016/j.biomaterials.2020.120614
44. Li X, Qi M, Sun X, et al. Surface treatments on titanium implants via nanostructured ceria for antibacterial and anti-inflammatory capabilities. *Acta Biomater*. 2019;94:627–643. doi:10.1016/j.actbio.2019.06.023
45. Wang Y, Li C, Wan Y, et al. Quercetin-loaded ceria nanocomposite potentiate dual-directional immunoregulation via macrophage polarization against periodontal inflammation. *Small*. 2021;17(41):e2101505. doi:10.1002/smll.202101505
46. Baldim V, Bedioui F, Mignet N, Margaill I, Berret JF. The enzyme-like catalytic activity of cerium oxide nanoparticles and its dependency on Ce(3+) surface area concentration. *Nanoscale*. 2018;10(15):6971–6980. doi:10.1039/C8NR00325D
47. Valodkar M, Rathore PS, Jadeja RN, Thounaojam M, Devkar RV, Thakore S. Cytotoxicity evaluation and antimicrobial studies of starch capped water soluble copper nanoparticles. *J Hazard Mater*. 2012;201–202:244–249. doi:10.1016/j.jhazmat.2011.11.077
48. Cheng G, Guo W, Han L, et al. Cerium oxide nanoparticles induce cytotoxicity in human hepatoma SMMC-7721 cells via oxidative stress and the activation of MAPK signaling pathways. *Toxicol in vitro*. 2013;27(3):1082–1088. doi:10.1016/j.tiv.2013.02.005
49. Wang L, Ai W, Zhai Y, Li H, Zhou K, Chen H. Effects of Nano-CeO_2 with different nanocrystal morphologies on cytotoxicity in HepG2 cells. *Int J Environ Res Public Health*. 2015;12(9):10806–10819. doi:10.3390/ijerph120910806
50. Mo J, Xie Q, Wei W, Zhao J. Revealing the immune perturbation of black phosphorus nanomaterials to macrophages by understanding the protein Corona. *Nat Commun*. 2018;9(1):2480. doi:10.1038/s41467-018-04873-7
51. Deng ZJ, Liang M, Monteiro M, Toth I, Minchin RF. Nanoparticle-induced unfolding of fibrinogen promotes Mac-1 receptor activation and inflammation. *Nature Nanotechnol*. 2011;6(1):39–44. doi:10.1038/nnano.2010.250
52. Ming P, Liu Y, Yu P, et al. A biomimetic Se-nHA/PC composite microsphere with synergistic immunomodulatory and osteogenic ability to activate bone regeneration in periodontitis. *Small*. 2024;20(9):e2305490. doi:10.1002/smll.202305490
53. Shao D, Li K, You M, et al. Macrophage polarization by plasma sprayed cerium coatings on titanium-based implants: cerium valence state matters. *Appl Surf Sci*. 2020;504:144070. doi:10.1016/j.apsusc.2019.144070
54. Xu J, Ding Y, Shi C, et al. Identification of cathepsin B as a therapeutic target for ferroptosis of macrophage after spinal cord injury. *Aging and Disease*. 2023;15(1):421–443. doi:10.14336/AD.2023.0509
55. Swanson KV, Deng M, Ting JP. The NLRP3 inflammasome: molecular activation and regulation to therapeutics. *Nat Rev Immunol*. 2019;19(8):477–489. doi:10.1038/s41577-019-0165-0
56. Lunov O, Uzhytchak M, Smolková B, et al. Remote actuation of apoptosis in liver cancer cells via magneto-mechanical modulation of iron oxide nanoparticles. *Cancers*. 2019;11(12):1873. doi:10.3390/cancers11121873
57. Mort JS, Buttle DJ. Cathepsin B. *Int J Biochem Cell Biol*. 1997;29(5):715–720. doi:10.1016/S1357-2725(96)00152-5
58. Rathinam VA, Vanaja SK, Waggoner L, et al. TRIF licenses caspase-11-dependent NLRP3 inflammasome activation by gram-negative bacteria. *Cell*. 2012;150(3):606–619. doi:10.1016/j.cell.2012.07.007
59. Rauner M, Sipos W, Pietschmann P. Osteoimmunology. *Int Arch Allergy Immunol*. 2007;143(1):31–48. doi:10.1159/000098223
60. Lv D, Li B, Liu Z, et al. ROS-mediated adaptation accelerates ecto-MSCs differentiation into osteoblasts. *Mol Med Rep*. 2024;30(6). doi:10.3892/mmr.2024.13365
61. Saxena Y, Routh S, Mukhopadhaya A. Immunoporosis: role of innate immune cells in osteoporosis. *Front Immunol*. 2021;12:687037. doi:10.3389/fimmu.2021.687037
62. Fischer V, Haffner-Luntzer M. Interaction between bone and immune cells: implications for postmenopausal osteoporosis. *Semin Cell Dev Biol*. 2022;123:14–21. doi:10.1016/j.semcdb.2021.05.014
63. Li YX, Zhang HY, Zhang Y, Cai DZ, Bai XC. The application of extracellular vesicles in orthopedic diseases. *Interdiscip Med*. 2024;2(3). doi:10.1002/INMD.20230055
64. Liu X, Wei Q, Sun J, et al. Small extracellular vesicles: yields, functionalization and applications in diabetic wound management. *Interdiscip Med*. 2023;1(4). doi:10.1002/INMD.20230019
65. Dou C, Ding N, Zhao C, et al. Estrogen deficiency-mediated M2 macrophage osteoclastogenesis contributes to M1/M2 ratio alteration in ovariectomized osteoporotic mice. *J Bone Miner Res*. 2018;33(5):899–908. doi:10.1002/jbmr.3364
66. McDonald MM, Khoo WH, Ng PY, et al. Osteoclasts recycle via osteomorphs during RANKL-stimulated bone resorption. *Cell*. 2021;184(5):1330–1347.e1313. doi:10.1016/j.cell.2021.02.002
67. Wang L, Chen K, Wan X, Wang F, Guo Z, Mo Z. NLRP3 inflammasome activation in mesenchymal stem cells inhibits osteogenic differentiation and enhances adipogenic differentiation. *Biochem Biophys Res Commun*. 2017;484(4):871–877. doi:10.1016/j.bbrc.2017.02.007
68. Sun X, Hao H, Han Q, et al. Human umbilical cord-derived mesenchymal stem cells ameliorate insulin resistance by suppressing NLRP3 inflammasome-mediated inflammation in type 2 diabetes rats. *Stem Cell Res Ther*. 2017;8(1):241. doi:10.1186/s13287-017-0668-1